Detection of doping atom distributions and individual dopants in InAs(110) by dynamic-mode scanning force microscopy in ultrahigh vacuum

A. Schwarz, W. Allers, U. D. Schwarz, and R. Wiesendanger
Institute of Applied Physics and Microstructure Research Center, University of Hamburg, Jungiusstrasse 11, D-20355 Hamburg, Germany
(Received 2 June 2000)

We investigate the influence of near-surface doping atoms of *in situ* cleaved *n*- and *p*-doped InAs(110) on images acquired with constant frequency shift by dynamic mode scanning force microscopy (DM-SFM) in ultrahigh vacuum. The local arrangement of doping atoms near the surface determines the distribution of mobile charge carriers and thus the electrostatic surface potential, which affects the contrast observed in DM-SFM images. The experiments reveal a strong dependence of the type and density of these charge carriers on the sign and magnitude of the applied bias voltage. Additionally, we find that the achieved resolution is directly related to the overlap of the screened Coulomb potential of ionized neighboring doping atoms. On *n*-InAs(110), the overlap is very strong, and the contrast observed in large-scale DM-SFM images acquired on atomically flat terraces reflects the density distribution of the doping atoms. The bias dependence of the contrast can be interpreted by the presence of an accumulation, depletion, or inversion zone underneath the probe tip. On a *p*-InAs(110) sample with a nearly identical doping concentration, however, a screened Coulomb potential around individual doping atoms could be detected, since the screening length is smaller than their mean distance between dopings. In atomically resolved images, charged doping atoms as well as charged As vacancies could be identified.

I. INTRODUCTION

Up to now, investigation of semiconducting samples performed in ultrahigh vacuum by means of dynamic mode scanning force microscopy, which is also called noncontact atomic force microscopy, focused mainly on their surface structure. Due to the high sensitivity of the frequency modulation technique, DM-SFM images acquired with a constant frequency shift provide topographical information down to the atomic scale (''true'' atomic resolution) on this type of samples.[1–9] In contrast, if electrostatic tip-sample forces are studied under UHV conditions, Kelvin probe force microscopy or electrostatic force microscopy are applied. Both techniques allow a spatially resolved measurement of charge distributions, band bending effects, or contact potential differences between two materials.[8,10–14]

However, DM-SFM itself is not exclusively sensitive to short-range atomic forces, which are usually associated with the topography of a sample. In this paper, we will demonstrate that on atomically flat semiconductors like *in situ* cleaved InAs(110), electrostatic interactions due to the presence of near-surface-ionized doping atoms can be directly observed (without applying any type of lock-in technique) in standard ''topographic'' DM-SFM images, i.e., in DM-SFM images acquired with constant frequency shift. Different aspects of contrast formation as well as bias dependence will be discussed. In particular, we will show that the resolution is strongly affected by the mean distance between neighboring doping atoms and the screening length in the material.

II. EXPERIMENTAL SETUP

The *n*- (sulfur) and *p*- (zinc) doped InAs single crystals (doping concentrations $N_D \approx 3\times10^{18}$ cm^{-3} and $N_A \approx (4–6)\times10^{18}$ cm^{-3}, respectively) used in this study were cleaved *in situ* parallel to the (110) surface in the preparation chamber of our UHV system at pressures below 1×10^{-7} Pa, and were then immediately transferred into the microscope located in the main chamber ($p<1\times10^{-8}$ Pa). The (110) surface of InAs is electrically neutral, and 1×1 relaxed, with a surface unit cell size of 0.606×0.427 nm^2.[15] The band gap has a width of 360 meV at room temperature. No intrinsic band bending occurs at the clean defect-free surface, and no surface states are present in the forbidden band gap.[16] The Fermi level is unpinned at the surface, and for our *n*-InAs (*p*-InAs) samples $\approx$290 meV ($\approx$18 meV) lies above (below) the conduction- (valence-) band edge. The electron gas is degenerated, even at 14 K,[17] where some experiments have been conducted on the *n*-doped material.

All measurements presented in this paper were made using our home-built ultrahigh-vacuum low-temperature scanning force microscope suitable for atomic resolution in the static and dynamic mode, which is described in detail elsewhere.[18] The instrument was operated in the dynamic mode, based on the frequency modulation technique introduced by Albrecht *et al.*,[19] keeping the vibration amplitude A constant while the frequency shift Δf between the eigenfrequency f_0 and the actual resonance frequency f of the cantilever are measured. The bias voltages U_{bias} are applied with respect to the grounded cantilever. For imaging, tips made from highly doped silicon (antimony, $N_D \approx 8\times10^{17}-5\times10^{18}$ cm^{-3}) were used.[20] These tips were cleaned by argon sputtering before the experiments on *n*-InAs(110), whereas they remained untreated for measurements on *p*-InAs(110). Eigenfrequencies of the free cantilevers were on the order of $f_0 \approx 170$ kHz, with spring constants around $k \approx 35$ N/m.

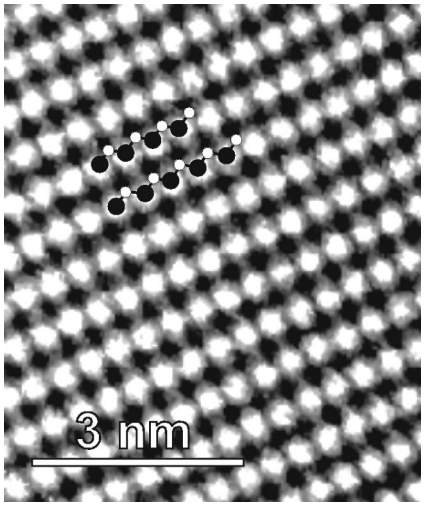

FIG. 1. Atomically resolved surface of *n*-InAs(110)-(1×1) imaged in the dynamic mode of scanning force microscopy with a constant frequency shift. The black and white circles in the upper left part indicate the positions of the As and In atoms, respectively. Due to the 1×1 relaxation, the surface is As terminated; consequently, protrusions correspond to the positions of the As atoms, while the In atoms do not show up in typical DM-SFM images (Ref. 9). Parameters: $T=14$ K, $k\approx 36$ N/m, $f_{\mathrm{res}}=160$ kHz, $A=\pm 12.7$ nm, image size 5.9×7.0 nm^2, $\Delta f=-60.5$ Hz, and $U_{\mathrm{bias}}=0$ V.

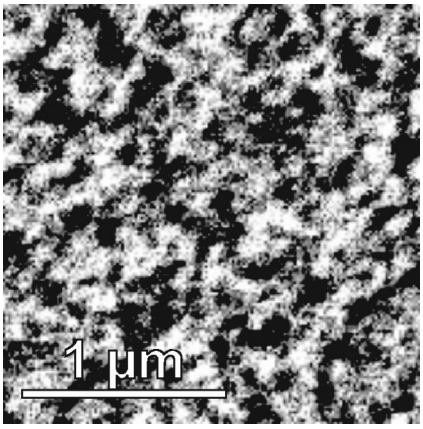

FIG. 2. Long-range contrast on a large-scale DM-SFM image acquired with a constant frequency shift on an atomically flat terrace of *n*-InAs(110). The image has been taken directly after cleavage under UHV conditions. The observed corrugation is of the order of 0.1–0.2 nm, and can be attributed to the presence of near-surface doping atoms, which lead to a locally varying electrostatic tip-sample interaction. Parameters: $T=300$ K, $k\approx 38$ N/m, $f_{\mathrm{res}}=177$ kHz, $A=\pm 10.2$ nm, image size 2.0×2.0 μm^2, $\Delta f=-62.5$ Hz, and $U_{\mathrm{bias}}=0$ V.

III. RESULTS

The cleaved *n*-InAs(110)-(1×1) surfaces exhibited large atomically flat terraces with distances of typically more than 1 μm between step edges. On atomic-scale images, we could clearly resolve the atomic structure with typical corrugations between 10 and 70 pm, as demonstrated in Fig. 1. The zigzag arrangement of As and In atoms at the surface is indicated by black and white circles, respectively. Typically, only the As atoms are visible as protrusions in DM-SFM images; further details on the atomic-scale imaging of *n*-InAs(110) with DM-SFM are given in Ref. 9. For the present needs, it is only important to mention that on *n*-doped material we did not observe any additional contrast in atomic-scale images besides the contrast caused by short-range atomic forces. On large-scale DM-SFM images, however, we found a long-range contrast with a corrugation of about 0.2 nm, as visible in Fig. 2.

To investigate the nature and origin of this contrast, we explored its bias dependence using the following technique. First, the tip-sample distance was stabilized at an image point with $\Delta f=-12.5$ Hz and $U_{\mathrm{bias}}=+0.50$ V. Then the feedback was switched off, and while the bias voltage was ramped in 10 s from -2.5 to $+3.5$ V, the frequency shift Δf was recorded. Applying this method at each image point of a regular raster, we could generate a series of Δf maps of the same surface area at different, but fixed, bias voltages. The four images displayed in Fig. 3 represent such Δf maps at $U_{\mathrm{bias}}=-2.22$, -0.25, $+0.50$, and $+2.75$ V. The encircled area illustrates the influence of the bias voltage: The contrast inverts from large negative to large positive bias voltages. At the stabilization voltage of $+0.50$ V, the contrast vanishes. This voltage was adjusted during DM-SFM images recorded before to obtain minimal overall contrast. This assures that the tip-sample distances are nearly identical at the beginning of each bias ramp.

In order to study this issue from a somewhat different point of view, we measured the effect of a bias ramp on the tip-sample distance with an active feedback, which keeps Δf constant (Fig. 4). Three regimes can be clearly distinguished in the resulting $z(U_{\mathrm{bias}})$ curve: For $U_{\mathrm{bias}}<-1.0$ V and $U_{\mathrm{bias}}>0.5$ V the tip-sample distance exhibits a stronger bias dependence than in between, where the curve is essentially flat. Furthermore, the curve is not symmetric with respect to $U_{\mathrm{bias}}=0$ V: The slope for $U_{\mathrm{bias}}>0.5$ V is approximately 10% smaller than for $U_{\mathrm{bias}}<1.0$ V.

On the *p*-InAs(110)-(1×1) surfaces investigated in this study, the situation was found to be quite different compared to the *n*-doped material, although the doping concentration was nearly the same. On large-scale DM-SFM images, circular white spots are visible. In Fig. 5, e.g., about 150 spots can be counted in an area of 14 400 nm^2. Closer analysis on the atomic scale (cf. Fig. 6) exhibits two different types of features, which we never observed on *n*-InAs. First, there are bright circular areas with diameters between 2 and 4 nm which possess an intact atomic structure. The upper line section in Fig. 6 along the [001] direction across such a bright area shows that the corrugation amplitude between the maxima remains constant, but the envelope has approximately a Gaussian shape. Second, there are dark areas with diameters around 3 nm. The corresponding lower line section in Fig. 6 reveals that one corrugation maximum is missing in the center of this dark area. The same holds for all regions, which appear depressed in Fig. 6.

IV. DISCUSSION

As a starting point of our discussion, we note that the distribution of bright and dark areas in the Figs. 2, 3, and 5 does not reflect topographic features, because cleaved InAs(110) is atomically flat, and under UHV conditions ad-

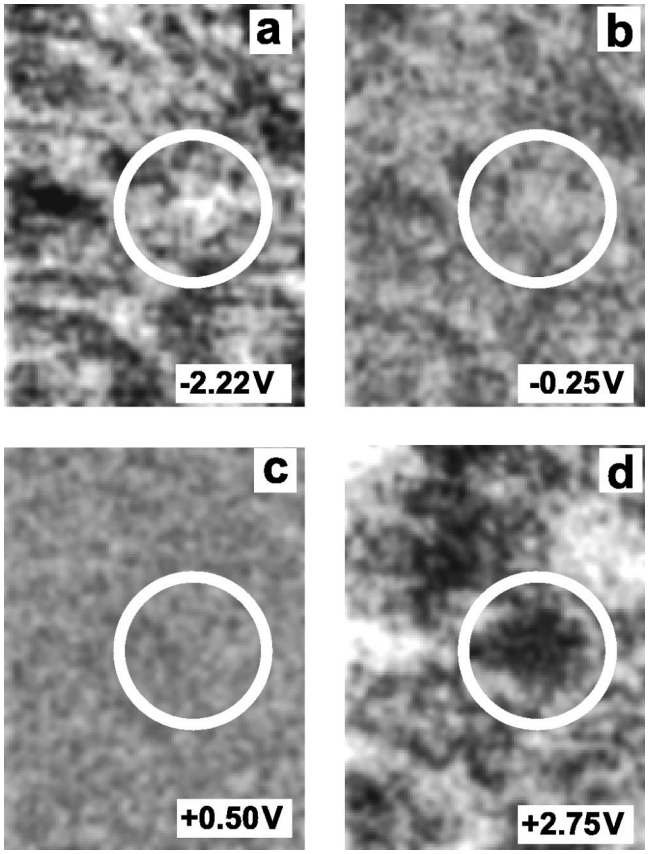

FIG. 3. Series of images demonstrating the bias dependence of the frequency shift at identical sample locations. A detailed description of the technique used to generate these images can be found in the text. The encircled area illustrates the bias-dependent contrast variations, which correspond to the fluctuations in the density distribution of doping atoms (cf. Sec. IV). (a) At $U_{\mathrm{bias}}=-2.22$ V, electrons (majority carriers) are accumulated at the surface. Bright areas correspond to a high density of doping atoms. (b) The contrast becomes weaker at smaller absolute values of U_{bias}. (c) At $U_{\mathrm{bias}}=+0.50$ V, the contrast vanishes. The surface is depopulated of mobile charge carriers. (d) At $U_{\mathrm{bias}}=+2.75$ V, holes (minority carriers) are generated near the surface. Inversion occurs and the contrast inverts. Parameters: $T=300$ K, $k\approx 37$ N/m, $f_{\mathrm{res}}=166$ kHz, $A=\pm 12.4$ nm, and image size 300×400 nm^2. The bias ramp at each point is performed between -2.5 and 3.0 V, with a 0.1-Hz sweep rate. The stabilization values at each point are: $\Delta f=-12.5$ Hz and $U_{\mathrm{offset}}=0.5$ V.

sorbates should not be present immediately after cleavage. Instead, the bias dependence of the contrast, as visible in the image series of Fig. 3, proves that the contrast is of electrostatic origin.

To understand the observed effects, the electrostatic properties of the tip-sample system have to be taken into account. For our purposes, the tips used in our experiments, although made from Si, can be considered to behave essentially as a metallic electrode. This is justified by the high doping level and, for untreated tips, by the high density of states in the Si band gap at the Si/SiO_2 interface.[21] For those tips, however, where the native oxide was removed by argon bombardment, a large number of defect states is induced into the Si band gap at the tip apex, which also ensures a metallic behavior.

The second electrode of the system is represented by the semiconducting InAs sample. Any potential difference between tip and sample results in an electric field, which is, in contrast to a metallic electrode, not compensated for within the first atomic layers of the InAs sample, but penetrates into the bulk. Therefore, the density of mobile charge carriers near the InAs surface is influenced in a more complex way by an electric field than it is in the metalliclike tip.[22] In this context, it is important to note that the potential difference between tip and sample is not only determined by the external applied bias voltage U_{bias}, but also depends on the difference between the work functions of tip (Φ_{tip}) and sample (Φ_{sample}). For our well-defined *n*- and *p*-InAs(110) samples,

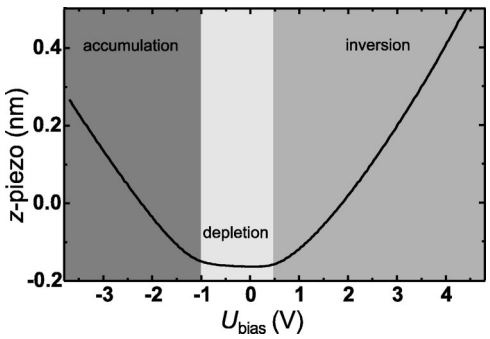

FIG. 4. $z(U_{\mathrm{bias}})$ curve on *n*-InAs acquired with an active feedback that keeps Δf constant. Three different regimes can be identified: accumulation at large negative bias voltages, depletion around 0 V, and inversion at large positive bias voltages. The flat regime in depletion indicates that electrons are pushed away from the surface. Parameters: $T=300$ K, $k\approx 38$ N/m, $f_{\mathrm{res}}=174$ kHz, $A=\pm 9.9$ nm, and $\Delta f=-17.5$ Hz.

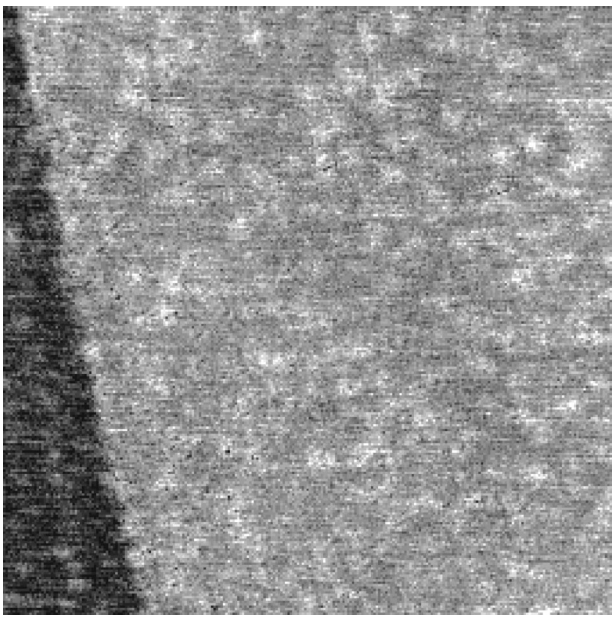

FIG. 5. Large-scale DM-SFM image of *p*-InAs with a monoatomic step on the left-hand side. The most prominent features are the approximately 150 bright spots. The analysis in Sec. IV reveals that these spots are caused by Coulomb potentials of individual near-surface doping atoms. Contrary to the situation found on *n*-InAs, the screened Coulomb potentials of neighboring doping atoms do not overlap due to their four times smaller screening length. Parameters: $T=300$ K, $k\approx 34$ N/m, $f_{\mathrm{res}}=149$ kHz, $A=\pm 15.3$ nm, image size 120×120 nm^2, $\Delta f=-110.0$ Hz, and $U_{\mathrm{bias}}=0$ V.

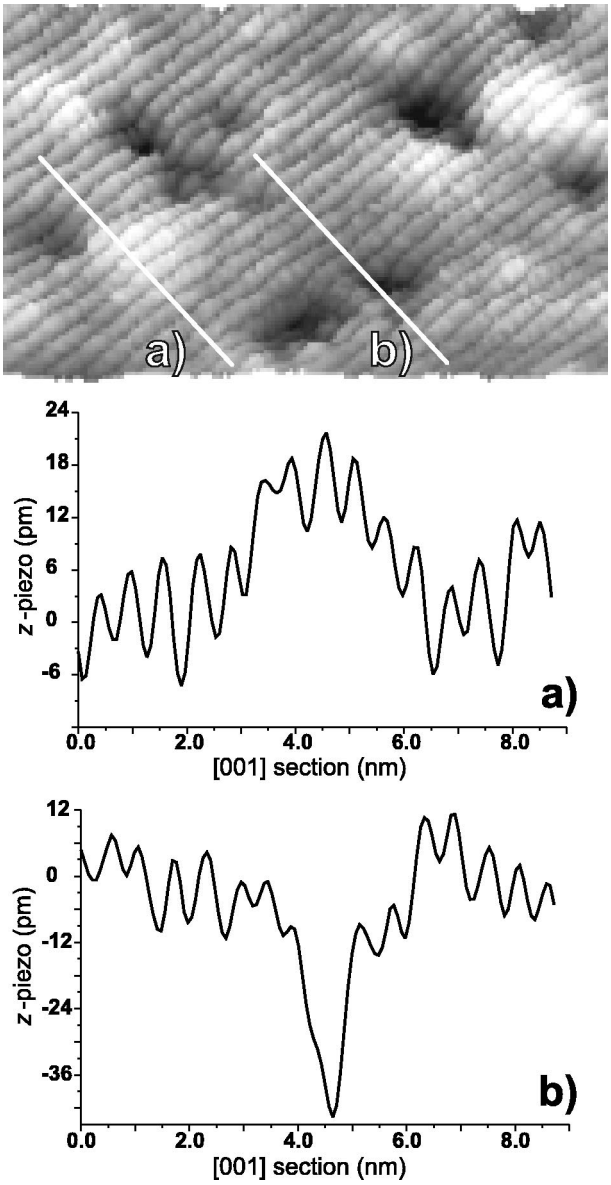

FIG. 6. Atomically resolved DM-SFM image of *p*-InAs(110) acquired with a constant frequency shift and displayed in a quasi-three-dimensional-representation. Bright areas with an intact atomic structure correspond to ionized (negatively charged) near-surface doping atoms (acceptors). They attract holes (majority carriers), and thereby the corrugation amplitudes appear elevated (a). Dark areas have at least one missing protrusion in their center (b), which can be identified as As vacancies. They are positively charged on *p*-InAs and repel holes. Parameters: $T=300$ K, $k\approx 34$ N/m, $f_{\mathrm{res}}=149$ kHz, $A=\pm 15.3$ nm, image size 16×10 nm^2, $\Delta f=-495.0$ Hz, and $U_{\mathrm{bias}}=0$ V.

the work functions can be easily determined, but Φ_{tip} is unknown, since the tip apex is not well defined at all.[23] However, for a qualitative analysis of our experimental results, it is not important to determine the absolute work function of the tip, but to realize that the potential difference is in general not zero at $U_{\mathrm{bias}}=0$ V. Let us now recall the effect of a potential difference on the band structure at the surface of a semiconductor.

For *n*-doped material, the electric field due to a negative potential with respect to the tip causes a downward band bending, which attracts majority carriers (electrons) toward the surface, i.e., an accumulation layer will form underneath the tip. At positive sample potentials, however, the bands bend upward, and electrons are repelled from the surface. If the conduction band crosses the Fermi level, no mobile charge carriers are available any longer at the surface, and a depletion layer emerges. At the transition from accumulation to depletion the band bending is zero, i.e., the flatband condition is realized. If $\Phi_{\mathrm{tip}}\neq\Phi_{\mathrm{sample}}$, zero band bending is not achieved at $U_{\mathrm{bias}}=0$, but at the so-called flatband voltage U_{FB}. The actual value of U_{FB} depends on the tip geometry as well as on the tip-sample distance.[24] Upon further upward band bending the depletion layer becomes thicker, until the valence band also crosses the Fermi level. At such a large positive potential difference, the depletion layer width remains constant, and minority carriers (holes) are generated near the surface, which lead to the formation of an inversion layer directly at the surface below the tip. For *p*-doped material, the mobile charge carriers behave in an analogous way.

The electrostatic interaction described above is always attractive, independent of the polarity of the charge carriers (electrons or holes), because the mirror charges induced in the tip are always of opposite polarity. The volume in which the band structure is influenced underneath the tip depends on the tip-sample distance as well as on the tip radius. Since the tip velocity during scanning and the oscillation frequency of the cantilever are much smaller than the response time of the electrons and holes in InAs, thermodynamic equilibrium is always maintained.[25]

With these considerations in mind, the contrast in Fig. 2, as well as the effect of the applied bias voltages in Figs. 3 and 4, can be explained. In the case of the $z(U_{\mathrm{bias}})$ curve of Fig. 4 the two regions with the strong bias dependence of the tip-sample distance indicate an increasing electrostatic interaction, which can be explained by the increasing density of charge carriers underneath the tip. Consequently, these two regimes can be attributed to the formation of an accumulation layer ($U_{\mathrm{bias}}<-1$ V) and an inversion layer ($U_{\mathrm{bias}}>0.5$ V), respectively, at the surface. The flat regime in between (-1.0 V$<U_{\mathrm{bias}}<0.5$ V) indicates depletion, i.e., the feedback keeps the tip-sample distance nearly constant, because the electrons are pushed into the bulk. Thereby, the distance between the tip and the electrons increases from -1.0 toward 0.5 V, which approximately compensates for the effect of the changing bias voltage, until minority carriers are generated at $U_{\mathrm{bias}}>0.5$ V. The 10% smaller slope in inversion is due to the additional capacitance of the depletion zone, which is not present in accumulation. Our interpretation is consistent with calculations done by Huang *et al.*[27] They found the same features for the force between a metallic electrode (tip) and a semiconducting electrode (sample) as visible in Fig. 4.

It is instructive to compare the complex behavior in Fig. 4 with $z(U_{\mathrm{bias}})$ curves taken on metallic tip-sample systems. Olsson *et al.*[26] found that on metallic systems such curves possess one pronounced minimum, and are symmetric with respect to that minimum. The voltage at the minimum is the contact potential voltage U_{CP} determined by the different work functions of the tip and sample. Due to the band-bending effects, the $z(U_{\mathrm{bias}})$ curve in Fig. 4 is neither symmetric nor does it possess a pronounced minimum. Conse-

quently, it is not possible to determine the contact potential U_{CP} from such curves. However, it is possible to roughly estimate the flatband voltage U_{FB} from such $z(U_{bias})$ curves. For *n*-type material the bands are flat when the slight upward band bending during depletion turns into a downward band bending in accumulation. In Fig. 4 this transition is marked by a strong increase of the tip-sample distance below approximately -1 V$=U_{FB}$.[28]

In order to explain the spatial variations of the contrast in our images (cf. Figs. 2 and 3), we have to point out that the absolute strength of the electrostatic interaction depends not only on extrinsic parameters such as the tip radius, the tip-sample distance, and the potential difference between tip and sample, but also on two intrinsic sample properties, namely, the doping concentration and the screening length. The role of these two important parameters is discussed in the following.

On a small enough scale, the distribution of the doping atoms fluctuates. This fluctuation explains the contrast in Fig. 2: bright and dark areas reflect high and low concentrations of mobile charge carriers, which directly scale with the local doping atom concentration. The contrast inversion in the image series presented in Fig. 3 illustrates how the observed contrast depends on the sign and magnitude of the applied bias voltage. The magnitude changes the number of charge carriers, while the sign determines the type of charge carriers present at the surface. In accumulation, the area underneath the tip is populated by electrons, which are attracted by the positively charged doping atoms. The increased density of electrons around doping atoms locally causes a stronger electrostatic tip-sample interaction, which in turn leads to a larger frequency shift. Therefore, bright areas in Fig. 3(a) at large negative bias voltages correspond to a relatively large concentration of near-surface doping atoms. Towards 0 V, the concentration of electrons decreases, and consequently the contrast diminishes [see Fig. 3(b)]. At the point of maximum depletion, approximately at $U_{bias}=0.5$ V, ionized doping atoms are the only charges present near the surface. Since they cannot be sufficiently screened by mobile charge carriers, the long-range electrostatic potentials overlap strongly and the contrast vanishes [see Fig. 3(c)]. Finally, at large positive voltages holes are generated underneath the tip. Since the holes are repelled by the positively charged doping atoms, the contrast reverses. Thus bright areas in Fig. 3(d) correspond to regions of reduced doping density.

The irregular shape of the long-range contrast in Figs. 2 and 3 shows that it is not possible to determine the exact position of individual doping atoms directly. This fits well with our finding that we never observed a contrast that could be attributed to the presence of near-surface doping atoms on atomic-scale images of *n*-InAs such as the one presented in Fig. 1. For *p*-InAs, however, the situation is different. In large-scale DM-SFM images, much more localized features are visible. In Fig. 5, e.g., we counted about 150 spots in an area of 120×120 nm^2. Assuming that each spot could be identified with one ionized doping atom, and taking the concentration of doping atoms given by the manufacturer, it follows that doping atoms up to a depth of 1.7–2.5 nm can be detected. But why should it be possible to detect single ionized doping atoms on *p*-InAs and not on *n*-InAs?

This question can be answered by taking a closer look at the second important intrinsic parameter mentioned above: the screening length λ_S. For degenerate semiconductors, λ_S can be calculated from

$$\lambda_S = 4(3/\pi)^{-1/6} N_{D,A}^{-1/6} \quad \epsilon^{-1/2} (m^*_{e,h}/m_e)^{-1/2} a_B{}^{1/2}, \quad (1)$$

where $a_B=0.053$ nm is the Bohr radius, $\epsilon=14.55$ the dielectric constant of InAs, and m_e is the mass of the free electron. $m^*_{e,h}$ represent the effective masses of the majority charge carriers (electrons and holes, respectively), and $N_{D,A}$ the concentration of either donator or acceptor doping atoms. Since both samples are degenerated, these values are identical to the majority-charge-carrier concentrations in thermal equilibrium. Note that λ_S depends only weakly on $N_{D,A}$, but strongly on the effective masses $m^*_{e,h}$. For InAs, the holes ($m^*_h=0.41m_e$) are about 16 times heavier than the electrons ($m^*_e=0.026m_e$), leading to a four times smaller screening length in *p*-InAs ($\lambda^p_S\approx2$ nm) than in *n*-InAs ($\lambda^n_S\approx8$ nm).

Let us now compare λ_S with the mean distance $\overline{r}$ between individual doping atoms. From the doping concentration, which is approximately the same in both samples ($N_D \approx 3\times10^{18}$ cm^{-3} and $N_A\approx4-6\times10^{18}$ cm^{-3}, respectively), we can calculate the mean distances to $\overline{r_D}\approx7$ nm for *n*-InAs and $\overline{r_A}\approx6$ nm for *p*-InAs. As a result, we see that there will be no significant overlap between the screened Coulomb potentials of neighboring doping atoms in *p*-InAs ($\lambda^p_S<\overline{r_A}$). Therefore, single doping atoms can be detected, as shown in Fig. 5. The number of spots counted on this image is in good agreement with the expected value, if one assumes that doping atoms up to a depth of the screening length influence the electrostatic potential at the surface.[29] In *n*-InAs, however, an average of six other doping atoms lie within a sphere of radius $R=\lambda^n_S$ around each doping atom, leading to a strong overlap between their screened Coulomb potentials. As a consequence, it is only possible to detect fluctuations in their distribution, but not individual doping atoms. We have to point out that the effect of the screening length on the resolution of individual doping atoms has to be separated from the influence of tip-radius and tip-sample distances.

With this knowledge, we are finally able to interpret the features observed in Fig. 6. The bright and dark areas, which are imaged simultaneously with the atomic structure of the *p*-InAs surface, can thus be attributed to enhanced or reduced electrostatic interactions, respectively. The electrostatic interaction corresponds to the distribution of the majority carriers (holes) at the surface, i.e., in bright (dark) areas the concentration of holes, is relatively large (small). Following this line of argument, each localized accumulation of holes (bright areas) can be explained by the existence of a negatively charged doping atom. This interpretation is supported by the radius of the bright areas, which are all smaller than or equal to λ^p_S, as expected from geometrical considerations. On the other hand, the localized depletion of holes (dark area) has to be induced by a localized positive charge. According to Ref. 9, missing protrusions, which are present in the center of the dark areas, can be identified as As vacancies. Scanning tunneling microscopy studies on *p*-InAs of the same doping concentration have shown that surface As vacancies are positively charged. Therefore, the dark areas can

be explained by the presence of positively charged As vacancies at the surface, surrounded by a region of reduced hole density.

V. SUMMARY

We investigated atomically flat *n*- and *p*-doped InAs(110) surfaces in ultrahigh vacuum with scanning force microscopy in the dynamic mode. On large-scale images spatial variations of the tip-sample interaction was observed. This nontopographic contrast is of electrostatic origin, and reflects the distribution of near-surface doping atoms. Its apparent bias dependence could be fully explained by the existence of accumulation, depletion, or inversion zones underneath the tip. The much smaller effective masses of the electrons in *n*-InAs compared to the effective masses of holes in *p*-InAs result in significantly different screening lengths on both materials. On *n*-InAs, the screening length of the Coulomb potentials around ionized near-surface doping atoms is larger than their mean distance for the doping concentrations chosen in our experiments, whereas the situation is the reverse on *p*-InAs. Consequently, on *n*-InAs only fluctuations in the distribution of near-surface doping atoms can be observed, while on *p*-InAs individual doping atoms can be identified. Finally, an analysis of atomic-scale images on *p*-InAs revealed that negatively charged doping atoms attract holes, in contrast to As vacancies, which repel holes due to their positive charge.

ACKNOWLEDGMENTS

The authors would like to thank Markus Morgenstern for helpful discussions. Financial support from the Deutsche Forschungsgemeinschaft (SFB 508 and SCHW 641/1-1), and the BMBF (Grant No. 13N7694/8) is gratefully acknowledged.

[1] F. J. Giessibl, Science **267**, 68 (1995).
[2] Y. Sugawara, M. Ohta, H. Ueyama, and S. Morita, Science **270**, 1646 (1995).
[3] R. Erlandsson, L. Olsson, and P. Martensson, Phys. Rev. B **54**, 8309 (1996).
[4] N. Nakagiri, M. Suzuki, K. Okiguchi, and H. Sugimura, Surf. Sci. **373**, 329 (1996).
[5] P. Güthner, Phys. Rev. B **54**, 8309 (1996).
[6] A. Schwarz, W. Allers, U. D. Schwarz, and R. Wiesendanger, Appl. Surf. Sci. **140**, 293 (1999).
[7] T. Uchihashi, Y. Sugawara, T. Tsukamoto, T. Minobe, S. Orisaka, T. Okada, and S. Morita, Appl. Surf. Sci. **140**, 304 (1999).
[8] Y. Sugawara, T. Uchihashi, M. Abe, and S. Morita, Appl. Surf. Sci. **140**, 371 (1999).
[9] A. Schwarz, W. Allers, U. D. Schwarz, and R. Wiesendanger, Phys. Rev. B **61**, 2837 (2000).
[10] A. Kikukawa, S. Hosaka, and R. Imura, Appl. Phys. Lett. **66**, 3510 (1995).
[11] A. Kikukawa, S. Hosaka, and R. Imura, Rev. Sci. Instrum. **67**, 1463 (1996).
[12] T. Uchihashi, M. Ohta, Y. Sugawara, Y. Yanase, T. Sigematsu, M. Suzuki, and S. Morita, J. Vac. Sci. Technol. B **15**, 1543 (1999).
[13] S. Kitamura and H. Iwatsuki, Appl. Phys. Lett. **72**, 3154 (1998).
[14] C. Sommerhalter, T. W. Matthes, T. Glatzel, A. Jäger-Waldau, and M. C. Lux-Steiner, Appl. Phys. Lett. **66**, 3510 (1999).
[15] C. B. Duke, C. Mailhot, A. Paton, D. J. Chadi, and A. Khan, J. Vac. Sci. Technol. B **3**, 1087 (1985).
[16] J. van Laar, A. Huijser, and T. L. van Rooy, J. Vac. Sci. Technol. **14**, 894 (1977).
[17] M. Morgenstern, C. Wittneven, R. Dombrowski, and R. Wiesendanger, Phys. Rev. Lett. **84**, 5588 (2000).
[18] W. Allers, A. Schwarz, U. D. Schwarz, and R. Wiesendanger, Rev. Sci. Instrum. **69**, 221 (1998).
[19] T. R. Albrecht, P. Grütter, D. Horne, and D. Rugar, J. Appl. Phys. **69**, 668 (1991).
[20] Nanosensors, Aidlingen, Germany.
[21] A detailed discussion on the electronic properties of Si/SiO_2 interfaces is, e.g., given by M. Schulz, in *Crystalline Semiconducting Materials and Devices*, edited by P. N. Butcher, N. H. March, and M. P. Tosi (Plenum Press, New York, 1986).
[22] S. Hudlet, M. Saint Jean, B. Roulet, J. Berger, and C. Guthmann, J. Appl. Phys. **77**, 3308 (1995).
[23] The work functions for our samples can be determined by the electron affinity and energy gap of InAs(110) [cf. G. W. Gobel and F. G. Allen, Phys. Rev. **137**, A245 (1965)], and by the position of the Fermi level, which can be calculated from N_A and N_D, respectively, $\Phi_{p\text{-InAs}} \approx 5.26$ eV and $\Phi_{n\text{-InAs}} \approx 4.61$ eV. Assuming a metalliclike tip apex, the Fermi level is expected to be near the valence band edge, which is 5.1 eV below the vacuum level. In Ref. 14 the authors found $\Phi_{\text{Si-tip}} \approx 4.7$ eV for an argon sputtered Si tip. However, the work function is very sensitive to the conditions at the tip apex as, e.g., tip radius and contaminations.
[24] Note that U_{FB} is not identical to the contact potential voltage U_{CP}, although both are related to the different work functions of tip and sample. The contact potential is defined by $U_{\text{CP}} = e(\Phi_{\text{tip}} - \Phi_{\text{sample}})$, where e is the electron charge. For an ideally metallic tip-sample system U_{CP} can be compensated for by an appropiate offset voltage $U_{\text{offset}} = -U_{\text{CP}}$.
[25] For typical mobilities of 33 000 $\text{cm}^2\,\text{V}^{-1}\,\text{s}^{-1}$ (*n*-InAs) and 420 $\text{m}^2\,\text{V}^{-1}\,\text{s}^{-1}$ (*p*-InAs), the response times are $\tau_n = 4.3 \times 10^{-13}$ s and $\tau_p = 9.6 \times 10^{-11}$ s, respectively. Note that other semiconductors might have much smaller response times.
[26] L. Olsson, N. Lin, V. Yakimov, and R. Erlandsson, J. Appl. Phys. **84**, 4060 (1998).
[27] Y. J. Huang, J. Slinkman, and C. C. Williams, Ultramicroscopy **42-44**, 298 (1992).
[28] Note that, due to the active feedback, the tip-sample distance is not constant during the measurement. However, the influence is rather small, since the total change in z is below 0.6 nm, while the electrostatic interaction is of long-range nature.
[29] Similar arguments were given in a scanning tunneling microscopy study of InAs, where the authors found that doping atoms located in depths of up to one times the screening length cause a detectable band bending: M. Morgenstern, D. Haude, V. Gudmundsson, C. Wittneven, R. Dombrowski, C. Steinebach, and R. Wiesendanger, J. Electron Microsc. Relat. Phenom. **109**, 127 (2000).